

Search for Lepton-Flavor-Violating and Lepton-Number-Violating $\tau \rightarrow \ell h h'$ Decay Modes

Y. Miyazaki,²⁴ I. Adachi,⁷ H. Aihara,⁴⁷ D. M. Asner,³⁵ V. Aulchenko,² T. Aushev,¹²
A. M. Bakich,⁴¹ A. Bay,¹⁹ V. Bhardwaj,²⁶ B. Bhuyan,⁸ M. Bischofberger,²⁶ A. Bozek,³⁰
M. Bračko,^{21,13} T. E. Browder,⁶ M.-C. Chang,⁴ A. Chen,²⁷ P. Chen,²⁹ B. G. Cheon,⁵
R. Chistov,¹² K. Cho,¹⁶ Y. Choi,⁴⁰ J. Dalseno,^{22,43} Z. Doležal,³ A. Drutskoy,¹²
S. Eidelman,² D. Epifanov,² J. E. Fast,³⁵ V. Gaur,⁴² N. Gabyshev,² A. Garmash,²
Y. M. Goh,⁵ J. Haba,⁷ H. Hayashii,²⁶ Y. Horii,²⁵ Y. Hoshi,⁴⁵ W.-S. Hou,²⁹ H. J. Hyun,¹⁸
T. Iijima,^{25,24} K. Inami,²⁴ A. Ishikawa,⁴⁶ R. Itoh,⁷ M. Iwabuchi,⁵³ Y. Iwasaki,⁷ T. Julius,²³
J. H. Kang,⁵³ C. Kiesling,²² H. J. Kim,¹⁸ H. O. Kim,¹⁸ K. T. Kim,¹⁷ M. J. Kim,¹⁸
Y. J. Kim,¹⁶ B. R. Ko,¹⁷ S. Koblitz,²² P. Kodyš,³ S. Korpar,^{21,13} P. Križan,^{20,13}
P. Krokovny,² A. Kuzmin,² Y.-J. Kwon,⁵³ S.-H. Lee,¹⁷ Y. Li,⁵¹ C.-L. Lim,⁵³ C. Liu,³⁸
Z. Q. Liu,⁹ D. Liventsev,¹² R. Louvot,¹⁹ D. Matvienko,² S. McOnie,⁴¹ K. Miyabayashi,²⁶
H. Miyata,³² R. Mizuk,¹² G. B. Mohanty,⁴² A. Moll,^{22,43} N. Muramatsu,³⁷ E. Nakano,³⁴
M. Nakao,⁷ S. Nishida,⁷ K. Nishimura,⁶ O. Nitoh,⁵⁰ S. Ogawa,⁴⁴ T. Ohshima,²⁴
S. Okuno,¹⁴ Y. Onuki,⁴⁷ P. Pakhlov,¹² G. Pakhlova,¹² C. W. Park,⁴⁰ H. K. Park,¹⁸
M. Petrič,¹³ L. E. Piilonen,⁵¹ M. Röhrken,¹⁵ S. Ryu,³⁹ H. Sahoo,⁶ Y. Sakai,⁷ T. Sanuki,⁴⁶
Y. Sato,⁴⁶ O. Schneider,¹⁹ C. Schwanda,¹¹ K. Senyo,⁵² O. Seon,²⁴ M. Shapkin,¹⁰
C. P. Shen,²⁴ T.-A. Shibata,⁴⁸ J.-G. Shiu,²⁹ B. Shwartz,² A. Sibidanov,⁴¹ F. Simon,^{22,43}
J. B. Singh,³⁶ P. Smerkol,¹³ Y.-S. Sohn,⁵³ A. Sokolov,¹⁰ E. Solovieva,¹² S. Stanič,³³
M. Starič,¹³ T. Sumiyoshi,⁴⁹ G. Tatishvili,³⁵ Y. Teramoto,³⁴ K. Trabelsi,⁷ T. Tsuboyama,⁷
M. Uchida,⁴⁸ S. Uehara,⁷ Y. Unno,⁵ S. Uno,⁷ P. Urquijo,¹ G. Varner,⁶ C. H. Wang,²⁸
P. Wang,⁹ E. Won,¹⁷ Y. Yamashita,³¹ Y. Yusa,³² Z. P. Zhang,³⁸ and V. Zhulanov²

(The Belle Collaboration)

¹*University of Bonn, Bonn, Germany*

²*Budker Institute of Nuclear Physics SB RAS and Novosibirsk State University,
Novosibirsk 630090, Russian Federation*

³*Faculty of Mathematics and Physics,
Charles University, Prague, The Czech Republic*

⁴*Department of Physics, Fu Jen Catholic University, Taipei, Taiwan*

⁵*Hanyang University, Seoul, South Korea*

⁶*University of Hawaii, Honolulu, HI, USA*

⁷*High Energy Accelerator Research Organization (KEK), Tsukuba, Japan*

⁸*Indian Institute of Technology Guwahati, Guwahati*

⁹*Institute of High Energy Physics, Chinese Academy of Sciences, Beijing, PR China*

¹⁰*Institute for High Energy Physics, Protvino, Russian Federation*

¹¹*Institute of High Energy Physics, Vienna, Austria*

¹²*Institute for Theoretical and Experimental Physics, Moscow, Russian Federation*

- ¹³*J. Stefan Institute, Ljubljana, Slovenia*
- ¹⁴*Kanagawa University, Yokohama, Japan*
- ¹⁵*Institut für Experimentelle Kernphysik,
Karlsruher Institut für Technologie, Karlsruhe, Germany*
- ¹⁶*Korea Institute of Science and Technology Information, Daejeon, South Korea*
- ¹⁷*Korea University, Seoul, South Korea*
- ¹⁸*Kyungpook National University, Taegu, South Korea*
- ¹⁹*École Polytechnique Fédérale de Lausanne, EPFL, Lausanne, Switzerland*
- ²⁰*Faculty of Mathematics and Physics,
University of Ljubljana, Ljubljana, Slovenia*
- ²¹*University of Maribor, Maribor, Slovenia*
- ²²*Max-Planck-Institut für Physik, München, Germany*
- ²³*University of Melbourne, Victoria, Australia*
- ²⁴*Graduate School of Science, Nagoya University, Nagoya, Japan*
- ²⁵*Kobayashi-Maskawa Institute, Nagoya University, Nagoya, Japan*
- ²⁶*Nara Women's University, Nara, Japan*
- ²⁷*National Central University, Chung-li, Taiwan*
- ²⁸*National United University, Miao Li, Taiwan*
- ²⁹*Department of Physics, National Taiwan University, Taipei, Taiwan*
- ³⁰*H. Niewodniczanski Institute of Nuclear Physics, Krakow, Poland*
- ³¹*Nippon Dental University, Niigata, Japan*
- ³²*Niigata University, Niigata, Japan*
- ³³*University of Nova Gorica, Nova Gorica, Slovenia*
- ³⁴*Osaka City University, Osaka, Japan*
- ³⁵*Pacific Northwest National Laboratory, Richland, WA, USA*
- ³⁶*Panjab University, Chandigarh, India*
- ³⁷*Research Center for Nuclear Physics, Osaka University, Osaka, Japan*
- ³⁸*University of Science and Technology of China, Hefei, PR China*
- ³⁹*Seoul National University, Seoul, South Korea*
- ⁴⁰*Sungkyunkwan University, Suwon, South Korea*
- ⁴¹*School of Physics, University of Sydney, NSW 2006, Australia*
- ⁴²*Tata Institute of Fundamental Research, Mumbai, India*
- ⁴³*Excellence Cluster Universe, Technische Universität München, Garching, Germany*
- ⁴⁴*Toho University, Funabashi, Japan*
- ⁴⁵*Tohoku Gakuin University, Tagajo, Japan*
- ⁴⁶*Tohoku University, Sendai, Japan*
- ⁴⁷*Department of Physics, University of Tokyo, Tokyo, Japan*
- ⁴⁸*Tokyo Institute of Technology, Tokyo, Japan*
- ⁴⁹*Tokyo Metropolitan University, Tokyo, Japan*
- ⁵⁰*Tokyo University of Agriculture and Technology, Tokyo, Japan*
- ⁵¹*CNP, Virginia Polytechnic Institute and State University, Blacksburg, VA, USA*
- ⁵²*Yamagata University, Yamagata, Japan*
- ⁵³*Yonsei University, Seoul, South Korea*

Abstract

We search for lepton-flavor-violating and lepton-number-violating τ decays into a lepton ($\ell =$ electron or muon) and two charged mesons ($h, h' = \pi^\pm$ or K^\pm) using 854 fb^{-1} of data collected with the Belle detector at the KEKB asymmetric-energy e^+e^- collider. We obtain 90% confidence level upper limits on the $\tau \rightarrow \ell hh'$ branching fractions in the range $(2.0 - 8.4) \times 10^{-8}$. These results improve upon our previously published upper limits by factors of about 1.8 on average.

PACS numbers: 11.30.Fs; 13.35.Dx; 14.60.Fg

INTRODUCTION

Lepton flavor violation (LFV) in charged lepton decays is forbidden in the Standard Model (SM) and highly suppressed even if neutrino mixing is taken into account. On the other hand, extensions of the SM, such as supersymmetry, leptoquark and many other models [1–8], predict LFV with branching fractions as large as 10^{-8} , which are accessible in current B -factory experiments. We search for neutrinoless lepton-flavor-violating $\tau^- \rightarrow \ell^- h^+ h'^-$ decays and lepton-number-violating $\tau^- \rightarrow \ell^+ h^- h'^-$ decays^[*], where ℓ is an electron or muon and $h^{(\prime)}$ is a charged pion or kaon. We analyse a 854 fb^{-1} data sample collected with the Belle detector [9] at the KEKB asymmetric-energy e^+e^- collider [10] at center-of-mass (CM) energies at or below the $\Upsilon(4S)$ and $\Upsilon(5S)$ resonances. Previously, we obtained 90% confidence level (C.L.) upper limits on the branching fractions using 671 fb^{-1} of data; the results were in the range $(3.3\text{--}16) \times 10^{-8}$ [11]. The BaBar collaboration has also published 90% C.L. upper limits in the range $(7\text{--}48) \times 10^{-8}$ using 221 fb^{-1} of data [12].

The Belle detector is a large-solid-angle magnetic spectrometer that consists of a silicon vertex detector (SVD), a 50-layer central drift chamber (CDC), an array of aerogel threshold Cherenkov counters (ACC), a barrel-like arrangement of time-of-flight scintillation counters (TOF), and an electromagnetic calorimeter comprised of CsI(Tl) crystals (ECL), all located inside a superconducting solenoid coil that provides a 1.5 T magnetic field. An iron flux-return located outside of the coil is instrumented to detect K_L^0 mesons and to identify muons (KLM). The detector is described in detail elsewhere [9].

Particle identification is very important for this measurement. We use particle identification likelihood variables based on the ratio of the energy deposited in the ECL to the momentum measured in the SVD and CDC, shower shape in the ECL, the particle's range in the KLM, hit information from the ACC, dE/dx measured in the CDC, and the particle's time of flight. To distinguish hadron species, we use likelihood ratios, $\mathcal{P}(i/j) = \mathcal{L}_i/(\mathcal{L}_i + \mathcal{L}_j)$, where \mathcal{L}_i (\mathcal{L}_j) is the likelihood of the observed detector response for a track with flavor i (j). For lepton identification, we form likelihood ratios $\mathcal{P}(e)$ [13] and $\mathcal{P}(\mu)$ [14] using the responses of the appropriate subdetectors.

We use Monte Carlo (MC) samples to estimate the signal efficiency and optimize the event selection. Signal and background event samples from generic $\tau^+\tau^-$ decays are generated by KKMC/TAUOLA [15]. For signal, we generate the $e^+e^- \rightarrow \tau^+\tau^-$ process, in which one τ is forced to decay into a lepton and two charged mesons using a three-body phase space model, while the other τ decays following SM branching ratios. Background samples from $B\bar{B}$ and continuum $e^+e^- \rightarrow q\bar{q}$ ($q = u, d, s, c$) processes are generated by EvtGen [16] while Bhabha and two-photon processes are generated by BHLUMI [17] and AAFH [18], respectively. In what follows, all kinematic variables are calculated in the laboratory frame unless otherwise specified. In particular, variables calculated in the e^+e^- CM frame are indicated by the superscript “CM.”

[*] Throughout this paper, charge-conjugate modes are implied; hence, the notation $\tau \rightarrow \ell h h'$ includes both $\tau^- \rightarrow \ell^- h^+ h'^-$ and $\tau^+ \rightarrow \ell^+ h^- h'^+$ modes.

EVENT SELECTION

We search for $\tau^+\tau^-$ events in which one τ (the signal τ) decays into a lepton and two charged mesons ($h, h' = \pi^\pm$ or K^\pm), and the other τ (the tag τ) decays into one charged track, any number of additional photons and neutrinos.

For each candidate event we calculate the $\ell hh'$ invariant mass ($M_{\ell hh'}$) and the difference of the $\ell hh'$ energy from the beam energy in the CM frame (ΔE). In the two-dimensional distribution of $M_{\ell hh'}$ versus ΔE , signal events should have $M_{\ell hh'}$ close to the τ -lepton mass (m_τ) and ΔE close to zero. From MC simulations, the dominant background for the $\tau \rightarrow \mu hh'$ modes is from continuum and generic $\tau^+\tau^-$ processes, while that for the $\tau \rightarrow e hh'$ modes is from two-photon processes. Therefore, the event selection is optimized mode-by-mode since the backgrounds are mode dependent.

Candidate τ -pair events are required to have four tracks with zero net charge. All charged tracks and photons are required to be reconstructed within the fiducial volume defined by $-0.866 < \cos \theta < 0.956$, where θ is the polar angle with respect to the direction along the e^+ beam. Each charged track should have transverse momentum (p_t) greater than 0.1 GeV/ c while each photon should have energy (E_γ) greater than 0.1 GeV. For each charged track, the distance of the closest point with respect to the interaction point is required to be less than 0.5 cm in the transverse direction and less than 3.0 cm in the longitudinal direction.

Using the plane perpendicular to the CM thrust axis [19], which is calculated from the observed tracks and photon candidates, we separate the particles in an event into two hemispheres. These are referred to as the signal and tag sides. The tag side is required to include a single charged track while the signal side is required to contain three charged tracks. We require one of three charged tracks on the signal side to be identified as a lepton. The electron and muon identification criteria are $\mathcal{P}(e) > 0.9$ with momentum $p > 0.6$ GeV/ c and $\mathcal{P}(\mu) > 0.95$ with $p > 1.0$ GeV/ c , respectively. In order to take into account the emission of bremsstrahlung photons from the electron, the momentum of the electron candidate is reconstructed by adding to it the momentum of every photon within 0.05 radians of the electron track direction. The electron (muon) identification efficiency is 91% (85%) while the probability to misidentify a pion as an electron (a muon) is below 0.5% (2%).

Charged kaons are identified by a condition $\mathcal{P}(K/\pi) > (0.6 - 0.9)$ for each mode, as shown in Table I, while charged pions are identified by the requirement $\mathcal{P}(K/\pi) < 0.6$. Furthermore, we apply a proton veto for kaon candidates, $\mathcal{P}(p/K) < 0.6$, to reduce protons incorrectly identified as kaons. The kaon (pion) identification efficiency is around 80% (88%) while the probability to misidentify a pion (kaon) as a kaon (pion) is below 10% (12%). In order to suppress background from photon conversions (*i.e.* $\gamma \rightarrow e^+e^-$), we require each h or h' candidate track to have $\mathcal{P}(e) < 0.1$. Furthermore, we apply the condition $\mathcal{P}(\mu) < 0.1$ to suppress two-photon background from $e^+e^- \rightarrow e^+e^-\mu^+\mu^-$.

To ensure that the missing particles are neutrinos rather than photons or charged particles that leave the detector acceptance, we impose requirements on the missing momentum \vec{p}_{miss} , which is calculated by subtracting the vector sum of the momenta of all tracks and photons from the sum of the e^+ and e^- beam momenta. We require that $|p_{\text{miss}}^t|$, the magnitude of the transverse component of \vec{p}_{miss} , be greater than 0.5 GeV/ c (0.7 GeV/ c) for the $\tau \rightarrow \mu hh'$ (ehh') modes, and that its direction point into the fiducial volume of the detector. For the $\tau^- \rightarrow e^-\pi^+\pi^-$ mode only, we apply the tighter selection requirement $|p_{\text{miss}}^t| > 1.5$ GeV/ c . To reject continuum, Bhabha and $\mu^+\mu^-$ background, we require the magnitude of the thrust (T) to be in the ranges given in Table I.

TABLE I: Selection criteria for kaon identification $\mathcal{P}(K/\pi)$ and magnitude of thrust (T).

Mode	$\mathcal{P}(K/\pi)$	T
$\tau \rightarrow \mu\pi\pi$	—	$0.90 < T < 0.98$
$\tau \rightarrow \mu K\pi$	> 0.9	$0.92 < T < 0.98$
$\tau \rightarrow \mu K K$	> 0.8	$0.92 < T < 0.98$
$\tau \rightarrow e\pi\pi$	—	$0.90 < T < 0.97$
$\tau \rightarrow e K\pi$	> 0.8	$0.90 < T < 0.97$
$\tau \rightarrow e K K$	> 0.6	$0.90 < T < 0.98$

To suppress the $B\bar{B}$ and continuum background, we require that the number of photons on the tag side be $n_{\gamma}^{\text{TAG}} \leq 2$ and $n_{\gamma}^{\text{TAG}} \leq 1$ for decays with hadronic and leptonic tags, respectively. A leptonic tag is defined as $\mathcal{P}(e) > 0.1$ or $\mathcal{P}(\mu) > 0.1$ while a tag is hadronic if the leptonic requirements are not satisfied. We allow at most one additional photon on the signal side. The reconstructed mass of the tag side, combining the photons with the charged track (assumed to be a pion mass) from the tag side, m_{tag} , is required to be less than 1.0 GeV/ c^2 to reduce the continuum background.

Since neutrinos are emitted on the tag side only, the direction of \vec{p}_{miss} should lie within the tag side of the event. The cosine of the opening angle between \vec{p}_{miss} and the charged track on the tag side in the CM system, $\cos\theta_{\text{tag-miss}}^{\text{CM}}$, is required to be greater than zero. If the track on the tag side is a hadron, we also require $\cos\theta_{\text{tag-miss}}^{\text{CM}} < 0.85$ for the $\tau \rightarrow \mu hh'$ modes. This requirement reduces continuum background with missing energy due to neutrons or K_L^0 's since the masses of the neutron and K_L^0 are larger than that of the neutrino. We also require that $\cos\theta_{\text{tag-miss}}^{\text{CM}} < 0.96$ for $\tau \rightarrow ehh'$ modes. This requirement reduces Bhabha, inelastic vector meson-photoproduction, and two-photon background, since radiated photons from the tag-side track result in missing momentum if they overlap with the ECL clusters associated with the tag-side track [20].

Photon conversions can result in large backgrounds when an electron is reconstructed as a hadron and still passes the electron veto. For the $\tau \rightarrow ehh'$ modes, the e^-h^+ and h'^-h^+ invariant masses for the $\tau^- \rightarrow e^-h^+h'^-$ modes (e^+h^- and $e^+h'^-$ for the $\tau^- \rightarrow e^+h^-h'^-$ modes), assigning the electron mass to both tracks, are required to be greater than 0.2 GeV/ c^2 to reduce photon conversion and other backgrounds.

For the $\tau \rightarrow \mu hh'$ modes, a real muon track can come from a kaon decaying in the CDC ($K^\pm \rightarrow \mu^\pm \nu_\mu$). Therefore, we apply a kaon veto, $\mathcal{P}(K/\pi) < 0.6$, for muon candidate tracks if the tag side track is a hadron (see Fig. 1 (a)). Another significant continuum background is from di-baryon production with a proton on the tag side. To suppress this background, we apply a proton veto, $\mathcal{P}(p/\pi) < 0.6$ and $\mathcal{P}(p/K) < 0.6$, as shown in Figs. 1 (b) and (c).

For the $\tau^- \rightarrow \mu^- \pi^+ \pi^-$ mode, we reduce the $e^+e^- \rightarrow \mu^+ \mu^- \gamma$ background (with the photon converting into an electron-positron pair) by requiring that the invariant mass of the pion pair, evaluated by assuming the electron mass for both tracks, exceed 0.2 GeV/ c^2 . In addition, we require the momentum of a muon in the CM system be less than 4.0 GeV/ c and $\cos\theta_{\text{tag-miss}}^{\text{CM}} < 0.97$ if the track is a muon candidate with $\mathcal{P}(\mu) > 0.1$.

For the $\tau \rightarrow \ell \pi K$ modes, the background in the signal region is from $\tau^- \rightarrow \pi^- \pi^+ \pi^- \nu_\tau$ events in which both the kaon and lepton candidates are misidentified. To reduce this background, we require the invariant mass of the three charged tracks on the signal side, $M_{\pi\pi\pi}$, reconstructed by assigning the pion mass to the tracks, be larger than 1.52 GeV/ c^2 .

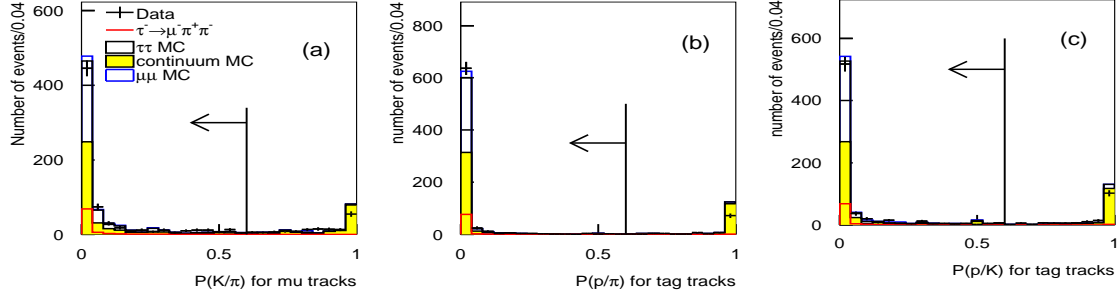


FIG. 1: (a) $\mathcal{P}(K/\pi)$ for muon tracks, (b) $\mathcal{P}(p/\pi)$ and (c) $\mathcal{P}(p/K)$ for hadronic tags, for $\tau^- \rightarrow \mu^- \pi^+ \pi^-$ candidate events. Signal MC ($\tau^- \rightarrow \mu^- \pi^+ \pi^-$) distributions are normalized arbitrarily while the background MC distributions are normalized to the data luminosity. The selected regions are indicated by arrows.

(see Fig.2).

Finally, to suppress backgrounds from generic $\tau^+ \tau^-$ and continuum processes, we apply a selection based on the magnitude of the missing mass squared m_{miss}^2 . The variable m_{miss}^2 is defined as $E_{\text{miss}}^2 - p_{\text{miss}}^2$, where $E_{\text{miss}} = E_{\text{total}} - E_{\text{vis}}$, E_{total} is the sum of the beam energies and E_{vis} is the total visible energy. We apply different selection criteria depending on the type of a one-prong tag: there should be two emitted neutrinos (a single missing neutrino) if the tagging track is leptonic (hadronic). For the $\tau \rightarrow e h h'$, $\mu \pi \pi$ and $\mu K K$ modes, we impose the requirements $-1.5 (\text{GeV}/c^2)^2 < m_{\text{miss}}^2 < 1.5 (\text{GeV}/c^2)^2$ for the hadronic tag and $-1.0 (\text{GeV}/c^2)^2 < m_{\text{miss}}^2 < 2.5 (\text{GeV}/c^2)^2$ for the leptonic tag. For the $\tau \rightarrow \mu \pi K$ modes, where the residual background after all selections is larger than in other modes, we require the following relation between p_{miss} and m_{miss}^2 : $p_{\text{miss}} > -8.0 \times m_{\text{miss}}^2 - 0.5$ and $p_{\text{miss}} > 8.0 \times m_{\text{miss}}^2 - 0.5$ for the hadronic tag and $p_{\text{miss}} > -9.0 \times m_{\text{miss}}^2 + 0.4$ and $p_{\text{miss}} > 1.8 \times m_{\text{miss}}^2 - 0.4$ for the leptonic tag; here p_{miss} is in GeV/c and m_{miss}^2 is in GeV/c^2 (see Fig. 3). Typically, 75% of the generic $\tau^+ \tau^-$ background is removed by these m_{miss}^2 requirements while 75% of the signal events are retained.

SIGNAL AND BACKGROUND ESTIMATION

For all modes, the $M_{\ell h h'}$ and ΔE resolutions are obtained from fits to the signal MC distributions, using an asymmetric Gaussian function that takes into account initial-state radiation. These Gaussians have widths as shown in Table II.

To evaluate the branching fractions, we use elliptical signal regions that contain $\pm 3\sigma$ of the MC signal satisfying all selection criteria. The ellipse is defined as

$$\frac{((M_{\ell h h'} - M_{\ell h h'}^0) \cos \theta - (\Delta E - \Delta E^0) \sin \theta)^2}{(3\sigma_{M_{\ell h h'}})^2} + \frac{((M_{\ell h h'} - M_{\ell h h'}^0) \sin \theta + (\Delta E - \Delta E^0) \cos \theta)^2}{(3\sigma_{\Delta E})^2} = 1 \quad (1)$$

where $M_{\ell h h'}^0$ and ΔE^0 are the coordinates of the center of the ellipse and $\sigma_{M_{\ell h h'}}$ ($\sigma_{\Delta E}$) is the average of $\sigma_{M_{\ell h h'}}^{\text{high}}$ and $\sigma_{M_{\ell h h'}}^{\text{low}}$ ($\sigma_{\Delta E}^{\text{high}}$ and $\sigma_{\Delta E}^{\text{low}}$) in Table II. These elliptical regions are determined by scanning $M_{\ell h h'}^0$, ΔE^0 and θ to maximize the significance in MC simulation

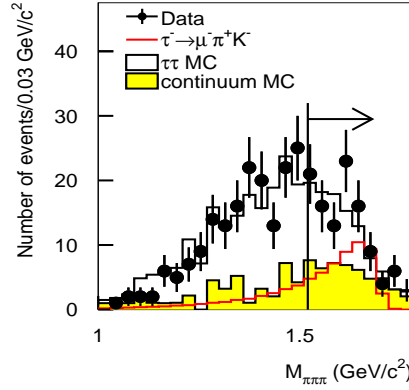


FIG. 2: Invariant mass distribution of three charged tracks on the signal side with the pion mass assigned to each track ($M_{\pi\pi\pi}$) for $\tau^- \rightarrow \mu^- \pi^+ K^-$ candidate events. Signal MC ($\tau^- \rightarrow \mu^- \pi^+ K^-$) distributions are normalized arbitrarily while the background MC distributions are normalized to the data luminosity. The selected regions are indicated by the arrow.

and obtain the highest sensitivity. Table III summarizes the signal efficiencies for each mode. We blind the data in the signal region until all selection criteria are finalized to avoid bias.

Figures 4 and 5 show scatter plots for data and signal MC samples distributed over a $\pm 20\sigma$ rectangular region in the $M_{\ell hh'} - \Delta E$ plane for the $\tau \rightarrow \mu hh'$ and $e hh'$ modes, respectively. For the $\tau \rightarrow \mu \pi \pi$ modes, the dominant background is from continuum processes while small background contributions come from generic $\tau^+ \tau^-$ events in the $\Delta E < 0$ GeV and $M_{\mu hh'} < m_\tau$ region, which are combinations of a misreconstructed muon and two pions. For the $\tau \rightarrow \mu KK$ modes, the dominant background sources are continuum and $\tau^+ \tau^-$ processes with a pion misidentified as a kaon. For the $\tau \rightarrow \mu \pi K$ modes, the dominant background is from generic $\tau^+ \tau^-$ decays with combinations of a misidentified muon, a misidentified kaon and a real pion from $\tau^- \rightarrow \pi^- \pi^+ \pi^- \nu$. If a pion is misidentified as a kaon, the reconstructed mass from generic $\tau^+ \tau^-$ background can be greater than the τ lepton mass since the kaon mass is greater than that of the pion. For the $\tau \rightarrow e hh'$ modes, the dominant background originates from two-photon processes, while the background from continuum and generic $\tau^+ \tau^-$ processes is small due to the low electron fake rate.

In order to estimate the background in the signal region, we use the number of data events observed in the sideband region inside a $\pm 5\sigma_{\Delta E}$ band around $\Delta E = 0$ GeV but excluding the signal region. The events in this band are projected onto the $M_{\ell hh'}$ axis. For the $\tau \rightarrow \mu \pi \pi$ modes, the extrapolation to the signal region is performed by fitting the sideband of the projected $M_{\mu \pi \pi}$ distribution using the sum of an exponential and a first-order polynomial function for generic $\tau\tau$ and continuum, respectively. For the $\tau \rightarrow e hh'$, μKK and $\mu \pi K$ modes, the background remaining after all selections is small, and extrapolation to the signal region assumes that the background is linear as a function of $M_{\ell hh'}$. An additional systematic uncertainty due to the estimation of the expected background includes the contributions due to the statistics of the background sample and the shape of the background distribution. By varying the assumptions about the background shape, we verify that this effect on the

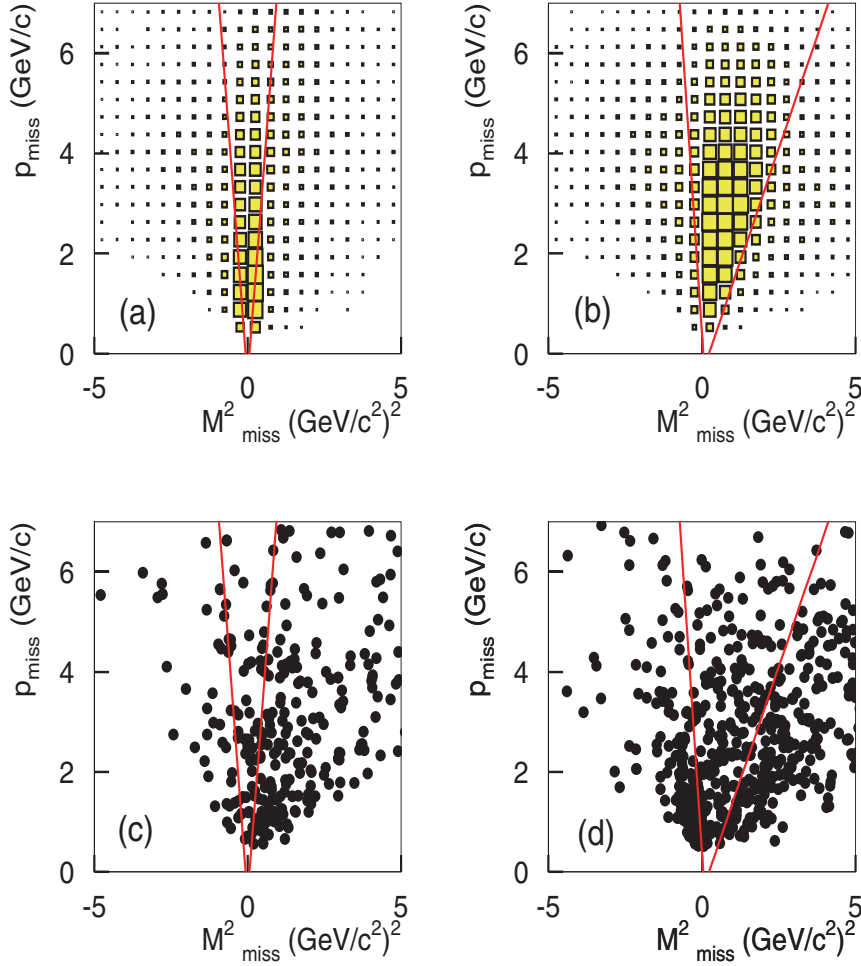


FIG. 3: Scatter plots of p_{miss} vs. m_{miss}^2 for $\tau^- \rightarrow \mu^- \pi^+ K^-$ modes. (a) and (c) show the signal MC ($\tau^- \rightarrow \mu^- \pi^+ K^-$) and generic $\tau^+ \tau^-$ MC distributions, respectively, for the hadronic tags while (b) and (d) show the same distributions for the leptonic tags. Selected regions are indicated by lines.

systematic uncertainty is less than 20% and is smaller than the background statistical error. The signal efficiency and the number of expected background events with its uncertainty, obtained by adding statistical and systematic uncertainties in quadrature for each mode, are summarized in Table III. After estimating the background, we open the blinded regions. We observe one candidate event for each of the $\tau^- \rightarrow \mu^+ \pi^- \pi^-$ and $\mu^- \pi^+ K^-$ modes, and no candidate events for the other modes. The numbers of events observed in the signal region are consistent with the expected background levels.

The dominant systematic uncertainties for this analysis come from the resolution in $M_{\ell hh'}$ and ΔE and from particle identification. We estimate the uncertainties from resolutions of $M_{\ell hh'}$ and ΔE due to the difference between data and MC samples to be (3.7-4.8)%. The uncertainties due to lepton identification are 2.2% and 1.9% from modes with an electron and a muon, respectively. The uncertainties due to hadron identification are 1.3% and 1.8% for pion and kaon candidates, respectively. The uncertainty due to the charged track finding is

TABLE II: Summary of $M_{\ell hh'}$ and ΔE resolutions ($\sigma_{M_{\ell hh'}}^{\text{high/low}}$ (MeV/ c^2) and $\sigma_{\Delta E}^{\text{high/low}}$ (MeV)). Here σ^{high} (σ^{low}) is the standard deviation on the higher (lower) side of the peak.

Mode	$\sigma_{M_{\ell hh'}}^{\text{high}}$	$\sigma_{M_{\ell hh'}}^{\text{low}}$	$\sigma_{\Delta E}^{\text{high}}$	$\sigma_{\Delta E}^{\text{low}}$
$\tau^- \rightarrow \mu^- \pi^+ \pi^-$	5.3	5.8	14.1	20.1
$\tau^- \rightarrow \mu^+ \pi^- \pi^-$	5.4	5.7	14.2	20.1
$\tau^- \rightarrow e^- \pi^+ \pi^-$	5.7	6.2	14.3	22.0
$\tau^- \rightarrow e^+ \pi^- \pi^-$	5.6	6.3	14.4	22.3
$\tau^- \rightarrow \mu^- K^+ K^-$	3.4	3.6	12.9	17.2
$\tau^- \rightarrow \mu^+ K^- K^-$	3.4	3.3	12.9	17.3
$\tau^- \rightarrow e^- K^+ K^-$	4.4	4.4	13.3	19.8
$\tau^- \rightarrow e^+ K^- K^-$	3.8	4.2	12.4	19.9
$\tau^- \rightarrow \mu^- \pi^+ K^-$	4.4	4.8	14.2	18.8
$\tau^- \rightarrow e^- \pi^+ K^-$	4.8	5.5	14.0	21.0
$\tau^- \rightarrow \mu^- K^+ \pi^-$	4.6	5.1	14.3	18.7
$\tau^- \rightarrow e^- K^+ \pi^-$	4.9	5.4	13.9	21.2
$\tau^- \rightarrow \mu^+ K^- \pi^-$	4.5	4.7	14.7	18.6
$\tau^- \rightarrow e^+ K^- \pi^-$	5.0	5.4	14.0	21.2

estimated to be 0.35% per charged track; therefore, the total uncertainty due to the charged track finding is 1.4%. The uncertainty due to integrated luminosity is estimated to be 1.4%. The uncertainties due to the trigger efficiency and MC statistics are negligible compared with the other uncertainties. All these uncertainties are added in quadrature, and the total systematic uncertainties for all modes are (3.8-4.7)%.

UPPER LIMITS ON THE BRANCHING FRACTIONS

Since no statistically significant excess of data over the expected background in the signal region is observed, we set upper limits on the branching fractions of the $\tau \rightarrow \ell hh'$ modes using the Feldman-Cousins method [21]. The 90% C.L. upper limit on the number of signal events including systematic uncertainty (s_{90}) is obtained using the POLE program without conditioning [22] based on the number of expected background events, the number of observed events and the systematic uncertainty. The upper limit on the branching fraction (\mathcal{B}) is then given by

$$\mathcal{B}(\tau \rightarrow \ell hh') < \frac{s_{90}}{2N_{\tau\tau}\varepsilon}, \quad (2)$$

where $N_{\tau\tau}$ is the number of $\tau^+\tau^-$ pairs, and ε is the signal efficiency. The value $N_{\tau\tau} = 782 \times 10^6$ is obtained from the integrated luminosity and the cross section of τ -pair production, which is calculated in KKMC [23] to be $\sigma_{\tau\tau} = 0.919 \pm 0.003$ nb and $\sigma_{\tau\tau} = 0.875 \pm 0.003$ nb for 782 fb^{-1} at $\Upsilon(4S)$ and 72 fb^{-1} at $\Upsilon(5S)$, respectively. Table III summarizes the results for all modes. The upper limits for the $\tau \rightarrow ehh'$ modes are in the range $(2.0 - 3.7) \times 10^{-8}$ while those for the $\tau \rightarrow \mu hh'$ modes are in the range $(2.1 - 8.6) \times 10^{-8}$. These results improve upon our previously published upper limits [11] by factors of about 1.8 on average. This

TABLE III: Summary of upper limits for each mode. The table shows the signal efficiency (ε), the number of expected background events (N_{BG}) estimated from the sideband data, the total systematic uncertainty (σ_{syst}), the number of observed events in the signal region (N_{obs}), 90% C.L. upper limit on the number of signal events including systematic uncertainties (s_{90}) and 90% C.L. upper limit on the branching fraction (\mathcal{B}) for each individual mode.

Mode	ε (%)	N_{BG}	σ_{syst} (%)	N_{obs}	s_{90}	\mathcal{B} (10^{-8})
$\tau^- \rightarrow \mu^- \pi^+ \pi^-$	5.83	0.63 ± 0.23	5.7	0	1.87	2.1
$\tau^- \rightarrow \mu^+ \pi^- \pi^-$	6.55	0.33 ± 0.16	5.6	1	4.01	3.9
$\tau^- \rightarrow e^- \pi^+ \pi^-$	5.45	0.55 ± 0.23	5.7	0	1.94	2.3
$\tau^- \rightarrow e^+ \pi^- \pi^-$	6.56	0.37 ± 0.19	5.5	0	2.10	2.0
$\tau^- \rightarrow \mu^- K^+ K^-$	2.85	0.51 ± 0.19	6.1	0	1.97	4.4
$\tau^- \rightarrow \mu^+ K^- K^-$	2.98	0.25 ± 0.13	6.2	0	2.21	4.7
$\tau^- \rightarrow e^- K^+ K^-$	4.29	0.17 ± 0.10	6.7	0	2.29	3.4
$\tau^- \rightarrow e^+ K^- K^-$	4.64	0.06 ± 0.06	6.5	0	2.39	3.3
$\tau^- \rightarrow \mu^- \pi^+ K^-$	2.72	0.72 ± 0.28	6.2	1	3.65	8.6
$\tau^- \rightarrow e^- \pi^+ K^-$	3.97	0.18 ± 0.13	6.4	0	2.27	3.7
$\tau^- \rightarrow \mu^- K^+ \pi^-$	2.62	0.64 ± 0.23	5.7	0	1.86	4.5
$\tau^- \rightarrow e^- K^+ \pi^-$	4.07	0.55 ± 0.31	6.2	0	1.97	3.1
$\tau^- \rightarrow \mu^+ K^- \pi^-$	2.55	0.56 ± 0.21	6.1	0	1.93	4.8
$\tau^- \rightarrow e^+ K^- \pi^-$	4.00	0.46 ± 0.21	6.2	0	2.03	3.2

improvement results both from using a larger data sample and from the introduction of an improved rejection of specific backgrounds, such as di-baryon production in the continuum for the $\tau \rightarrow \mu hh'$ modes, and improved kinematic event selections, for example, the $M_{\pi\pi\pi}$ requirement for the $\tau \rightarrow \ell\pi K$ modes.

SUMMARY

We have searched for lepton-flavor τ decays into a lepton and two charged mesons using 854 fb $^{-1}$ of data. We obtain 90% C.L. upper limits on the branching fractions of $\tau \rightarrow eh'h'$ in the range $(2.0 - 3.7) \times 10^{-8}$ and upper limits on $\tau \rightarrow \mu hh'$ in the range $(2.1 - 8.6) \times 10^{-8}$. These results improve upon our previously published upper limits by factors of about 1.8 on average. These more stringent upper limits can be used to constrain the space of parameters in various models of new physics.

Acknowledgments

We thank the KEKB group for the excellent operation of the accelerator; the KEK cryogenics group for the efficient operation of the solenoid; and the KEK computer group, the National Institute of Informatics, and the PNNL/EMSL computing group for valuable computing and SINET4 network support. We acknowledge support from the Ministry of Education, Culture, Sports, Science, and Technology (MEXT) of Japan, the Japan Society

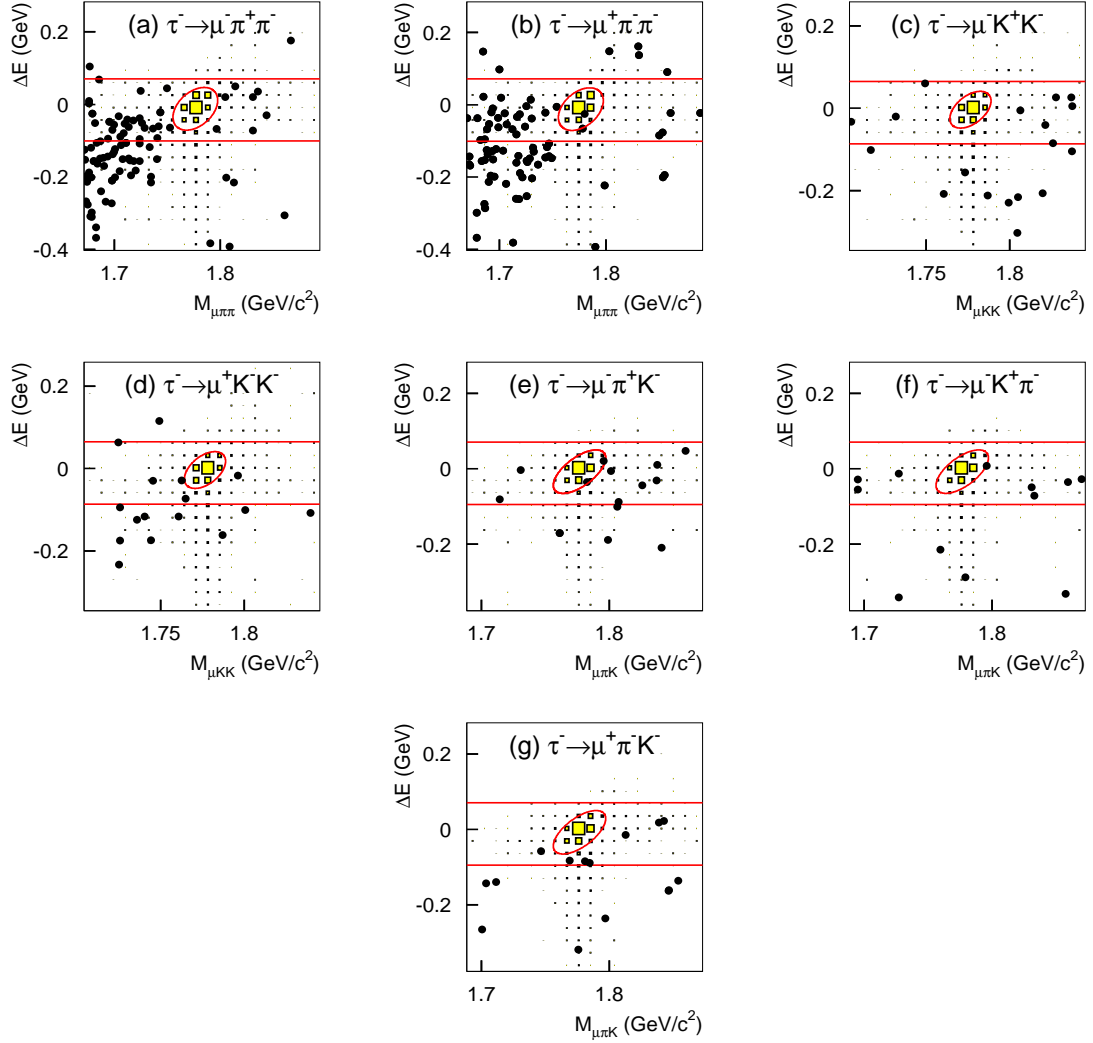


FIG. 4: Scatter plots in the $M_{\ell hh'} - \Delta E$ plane within a $\pm 20\sigma$ region for the (a) $\tau^- \rightarrow \mu^- \pi^+ \pi^-$, (b) $\tau^- \rightarrow \mu^+ \pi^- \pi^-$, (c) $\tau^- \rightarrow \mu^- K^+ K^-$, (d) $\tau^- \rightarrow \mu^+ K^- K^-$, (e) $\tau^- \rightarrow \mu^- \pi^+ K^-$, (f) $\tau^- \rightarrow \mu^- K^+ \pi^-$, and (g) $\tau^- \rightarrow \mu^+ \pi^- K^-$ modes. The data are indicated by the solid circles. The filled boxes show the MC signal distribution with arbitrary normalization. The elliptical signal regions shown by solid curves are used for evaluating the signal yield. The region between two horizontal solid lines excluding the signal region is used as a sideband.

for the Promotion of Science (JSPS), and the Tau-Lepton Physics Research Center of Nagoya University; the Australian Research Council and the Australian Department of Industry, Innovation, Science and Research; the National Natural Science Foundation of China under contract No. 10575109, 10775142, 10875115 and 10825524; the Ministry of Education, Youth and Sports of the Czech Republic under contract No. LA10033 and MSM0021620859; the Department of Science and Technology of India; the Istituto Nazionale di Fisica Nucleare of Italy; the BK21 and WCU program of the Ministry Education Science and Technology, National Research Foundation of Korea, and GSDC of the Korea Institute of Science and Technology Information; the Polish Ministry of Science and Higher Education; the Ministry

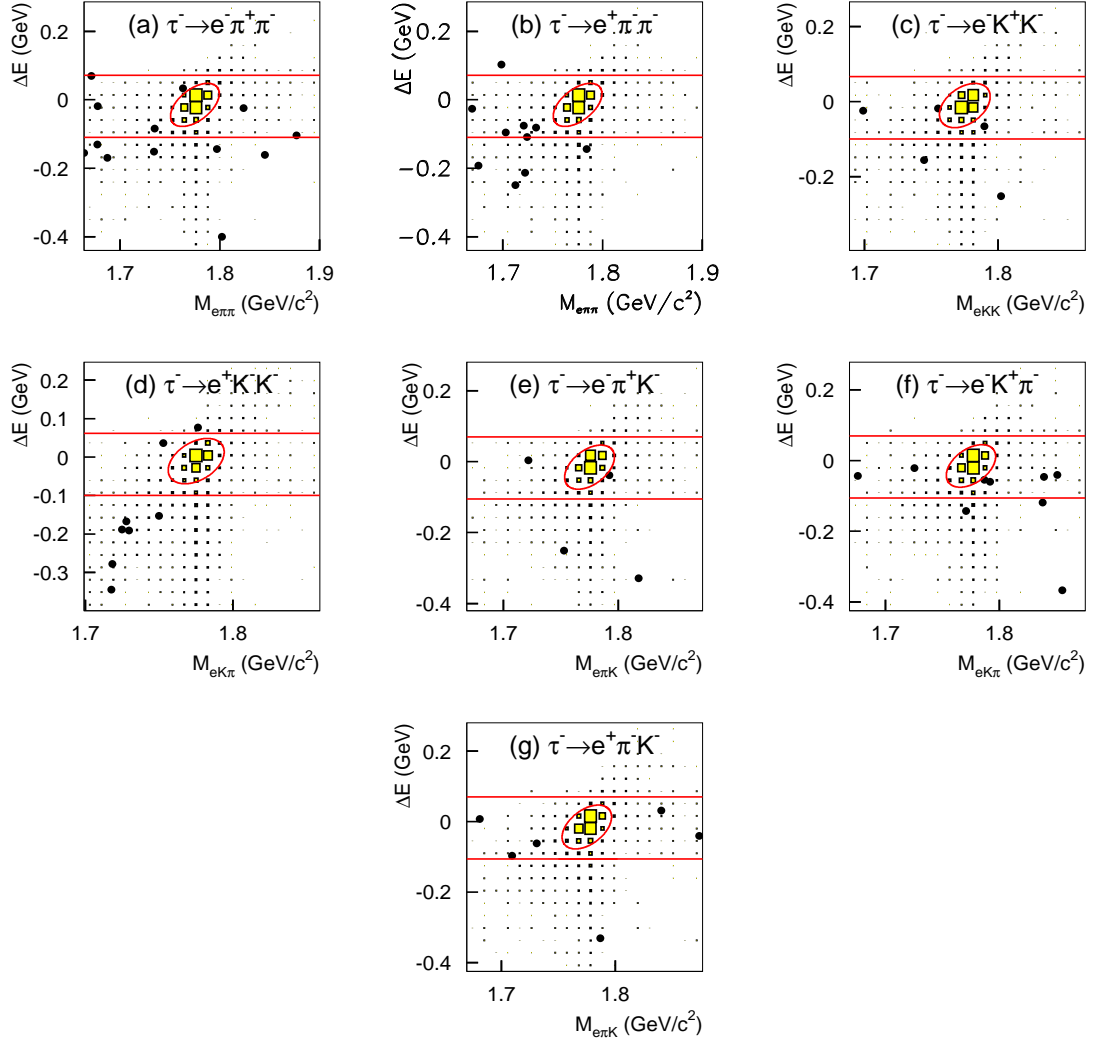


FIG. 5: Scatter plots in the $M_{\ell hh'} - \Delta E$ plane within a $\pm 20\sigma$ region for a (a) $\tau^- \rightarrow e^- \pi^+ \pi^-$, (b) $\tau^- \rightarrow e^+ \pi^- \pi^-$, (c) $\tau^- \rightarrow e^- K^+ K^-$, (d) $\tau^- \rightarrow e^+ K^- K^-$, (e) $\tau^- \rightarrow e^- \pi^+ K^-$, (f) $\tau^- \rightarrow e^- K^+ \pi^-$, and (g) $\tau^- \rightarrow e^+ \pi^- K^-$ modes. The data are indicated by the solid circles. The filled boxes show the MC signal distribution with arbitrary normalization. The elliptical signal regions shown by solid curves are used for evaluating the signal yield. The region between two horizontal solid lines excluding the signal region is used as a sideband.

of Education and Science of the Russian Federation and the Russian Federal Agency for Atomic Energy; the Slovenian Research Agency; the Swiss National Science Foundation; the National Science Council and the Ministry of Education of Taiwan; and the U.S. Department of Energy and the National Science Foundation. This work is supported by a Grant-in-Aid from MEXT for Science Research in a Priority Area (“New Development of Flavor Physics”), and from JSPS for Creative Scientific Research (“Evolution of Tau-lepton Physics”).

-
- [1] A. Ilakovac, Phys. Rev. D **62**, 036010 (2000).
- [2] D. Black *et al.*, Phys. Rev. D **66**, 053002 (2002).
- [3] C.-H. Chen and C.-Q. Geng, Phys. Rev. D **74**, 035010 (2006).
- [4] E. Arganda, M.J. Herrero and J. Portoles, JHEP **0806**, 079 (2008).
- [5] R. Benbrik and C. H. Chen, Phys. Lett. B **672**, 172 (2009).
- [6] Z. H. Li, Y. Li and H. X. Xu, Phys. Lett. B **677**, 150 (2009).
- [7] W. J. P. Li *et al.*, Int. J. Mod. Phys. A **25**, 4827 (2010).
- [8] W. Liu, C. X. Yue and J. Zhang, Eur. Phys. J. C **68**, 197 (2010).
- [9] A. Abashian *et al.* (Belle Collaboration), Nucl. Instr. and Meth. A **479**, 117 (2002).
- [10] S. Kurokawa and E. Kikutani, Nucl. Instr. and Meth. A **499**, 1 (2003), and other papers included in this Volume.
- [11] Y. Miyazaki *et al.* (Belle Collaboration), Phys. Lett. B **682**, 355 (2010).
- [12] B. Aubert *et al.* (BaBar Collaboration), Phys. Rev. Lett. **95**, 191801 (2005).
- [13] K. Hanagaki *et al.*, Nucl. Instr. and Meth. A **485**, 490 (2002).
- [14] A. Abashian *et al.*, Nucl. Instr. and Meth. A **491**, 69 (2002).
- [15] S. Jadach *et al.*, Comp. Phys. Commun. **130**, 260 (2000).
- [16] D. J. Lange, Nucl. Instr. and Meth. A **462**, 152 (2001).
- [17] S. Jadach *et al.*, Comp. Phys. Commun. **70**, 305 (1992).
- [18] F. A. Berends *et al.*, Comp. Phys. Commun. **40**, 285 (1986).
- [19] S. Brandt *et al.*, Phys. Lett. **12**, 57 (1964); E. Farhi, Phys. Rev. Lett. **39**, 1587 (1977).
- [20] K. Hayasaka *et al.* (Belle Collaboration), Phys. Lett. B **613**, 20 (2005).
- [21] G. J. Feldman and R. D. Cousins, Phys. Rev. D **57**, 3873 (1998).
- [22] See <http://www3.tsl.uu.se/~conrad/pole.html>; J. Conrad *et al.*, Phys. Rev. D **67**, 012002 (2003).
- [23] S. Banerjee *et al.*, Phys. Rev. D **77**, 054012 (2008).